Planta (2012) 235:713–727
DOI 10.1007/s00425-011-1532-7

ORIGINAL ARTICLE

OsLIS-L1 encoding a lissencephaly type-1-like protein with WD40 repeats is required for plant height and male gametophyte formation in rice

Xinqiang Gao · Zhihui Chen · Jian Zhang · Xingwang Li · Guoxing Chen · Xianghua Li · Changyin Wu

Received: 17 May 2011 / Accepted: 29 September 2011 / Published online: 22 October 2011

Abstract Although a large number of genes encoding the WD40 motif have been identified as being involved in various developmental processes in *Arabidopsis*, little is known about the function of these genes in rice (*Oryza sativa*). Here, we report the cloning and functional characterization of a novel rice gene *OsLIS-L1* (*Lissencephaly type-1-like 1*), which is required for normal fertility and the first internode elongation. *OsLIS-L1* encodes a lissencephaly type-1-like protein containing the WD40 motif that is required for brain development in human. SMART algorithm analysis indicated that OsLIS-L1 contains a LIS1 homology (LisH) domain, a C terminus to LisH (CTLH) domain, a five WD40-repeat domain in the middle, and a domain with four WD40 repeats which is homologous to the β subunit of trimeric G-proteins (G_{β}). *OsLIS-L1* transcript is relatively highly abundant in stem and panicle and has a dynamic expression pattern at different panicle developmental stages. Two independent alleles, designated *oslis-l1-1* and *oslis-l1-2*, exhibited similar abnormal developmental phenotypes, including semi-dwarf, shorter panicle length, and reduced male fertility. Cytological examination confirmed that *OsLIS-L1* does not affect the meiosis in pollen mother cells. Compared with wild type, the *oslis-l1* mutant had abnormal male gametophyte formation, but anther cell wall and pollen wall development were not affected. Histological analysis revealed that OsLIS-L1 regulates the cell proliferation in the first internode under the panicle. Our results indicate that *OsLIS-L1* plays an important role in male gametophyte formation and the first internode elongation in rice.

Keywords *Lissencephaly 1* (*LIS1*) · T-DNA · Rice · WD40 repeats · Male fertility · Plant height

Introduction

Lissencephaly 1 (*LIS1*) was the first gene identified in the pathogenesis of type-1 lissencephaly, a severe brain developmental disease characterized by mislocalization of cortical neurons (Reiner et al. 1993). The amino acid sequence of LIS1 is usually characterized as three distinct regions (Kim et al. 2004). The first region is the LIS1-homology (LisH) motif, which includes residues 1–39 at the N terminus and has recently been recognized as a novel ubiquitous motif that is widely found in 114 eukaryotic proteins (Emes and Ponting 2001). The second region is a coiled-coil region which contains the spanning amino acids 40–85. It was reported that LisH and the coiled-coil fragments were involved in homodimerization of the protein (Tai et al. 2002). Studies on LIS1-interacting proteins, either in human or in mouse models, have suggested that LIS1 may play a role in the pathogenesis of numerous diseases such as male sterility, schizophrenia, neuronal degeneration and viral infections (Reiner et al. 2006). The third distinct region of LIS1 is the WD40 (also known as Trp-Asp) motif, a stretch of approximately 40 amino acid that typically terminates in Trp-Asp (Neer et al. 1994). WD40 motifs usually present as 4–10 tandem repeats to form a functional structure. It was reported that repeated

Electronic supplementary material The online version of this article (doi:10.1007/s00425-011-1532-7) contains supplementary material, which is available to authorized users.

X. Gao · Z. Chen · J. Zhang · X. Li · G. Chen · X. Li · C. Wu (✉)
National Key Laboratory of Crop Genetic Improvement, National Center of Plant Gene Research (Wuhan), Huazhong Agricultural University, Wuhan 430070, China
e-mail: cywu@mail.hzau.edu.cn

WD40 motifs acted as a site for protein–protein interaction, and proteins containing WD40 repeats serve as platforms for the assembly of protein complexes or mediators of transient interplay among other proteins (Neer et al. 1994; Sondek et al. 1996).

WD40-repeat proteins not only play various key roles in plant biological process, such as signal transduction, cytoskeletal dynamics, protein trafficking, nuclear export, and RNA processing, but are also especially involved in chromatin modification and transcriptional mechanisms (van Nocker and Ludwig 2003). A recent plant study has revealed 85 and 78 WD40 motif-containing proteins in *Arabidopsis* and rice, respectively (Lee et al. 2008). A large number of genes encoding WD40 motif-containing proteins have been identified in *Arabidopsis*. For examples, the *CONSTITUTIVELY PHOTOMORPHOGENIC 1* (*COP1*) and *SUPPRESSOR OF PHYA-105* (*SPA1*) are involved in the light signaling/photomorphogenesis and flowering (Hoecker et al. 1999; Holm et al. 2002; von Arnim et al. 1997), respectively. *GTP BINDING PROTEIN BETA 1* (*AGB1*) is required for auxin response and cell division (Ullah et al. 2003). *FASCIATA2* (*FAS2*) is involved in meristem maintenance (Kaya et al. 2001). *LEUNIG* (*LUG*) function in floral development (Franks et al. 2002; Liu and Meyerowitz 1995). *FERTILIZATION-INDEPENDENT ENDOSPERM* (*FIE*) regulates seed development and flowering (Sorensen et al. 2001). *CYCLOPHILIN71* (*CYP71*), which interacts with histone H3, is essential for chromatin-based gene silencing and organogenesis (Li et al. 2007).

Although extensive studies have been carried out in *Arabidopsis*, the biological function of WD40 motif-containing genes has seldom been elucidated in depth in the monocot plant rice. One example from rice is *Rice Immature Pollen 1* (*RIP1*), which contained five conservative WD40 domains on its C terminus (Han et al. 2006) and is more highly expressed in anthers than in other tissues. During anther development, a high level of *RIP1* transcript accumulates in the late vacuolated and mature pollen stages. RIP1 loss-of-function causes not only abortive male gametophyte development, but also defects in pollen germination (Han et al. 2006). Another documented example of a rice WD40 motif-containing protein is the Salt Responsive WD40 protein (SRWD) subfamily. This gene subfamily can be phylogenetically divided into four groups and consists of five members in rice. Expression profile experiment results revealed that all five members were significantly up-regulated under salt stress, suggesting all of them play important function in salt response (Huang et al. 2008). However, the detailed biological functions of *SRWD* genes remain to be explored.

Molecular studies in *Arabidopsis* and rice have revealed that numerous genes are required for gametophyte generation. Because the cytological course of the embryo sac formation is more complicated than microsporogenesis and microgametogenesis, the roles of a majority of the genes related to fertility have been characterized during stamen and pollen development. In flowering plants, male reproductive development requires the differentiation of anther tissues and proper male meiosis to produce microspores (Ma 2005). Male gametophyte development in the anther compartment of the stamen depends on functional cross-talk between gametophytic and sporophytic tissues (Zhang and Wilson 2009). In the last few years, a number of genes controlling anther development, especially for the tapetum degeneration have been characterized in rice. The *UNDEVELOPED TAPETUM1* (*UDT1*) gene, encoding a bHLH transcription factor, is involved in tapetal cell differentiation in rice (Jung et al. 2005). *Tapetum Degeneration Retardation* (*TDR*), a putative homolog of *AMS* in *Arabidopsis*, is downstream of *UDT1* and plays a crucial role in tapetum degeneration and microspore development (Li et al. 2006; Zhang et al. 2008). It was reported that silencing the rice *UDP-Glucose Pyrophosphorylase 1* gene inhibits the degeneration of the tapetum (Chen et al. 2007). *Carbon Starved Anther* (*CSA*), encoding an R2R3 MYB transcription factor, controls sugar partitioning into the anther and is required for anther development and pollen maturation (Zhang et al. 2010). *CYP704B2*, a member cytochrome P450 family, is involved in catalyzing v-hydroxylation of C16 and C18 fatty acids and is required for anther cutin biosynthesis and pollen exine formation in rice (Li et al. 2010). *PERSISTENT TAPETAL CELL1* (*PTC1*), encodes a PHD-Finger protein, is a key regulator of tapetal programmed cell death and pollen development in rice (Li et al. 2011a). Rice MADS3 regulates ROS homeostasis during late anther development and is a key transcriptional regulator that functions in late anther development and pollen formation in rice (Hu et al. 2011). Recently, rice *APOPTOSIS INHIBITOR5* (*API5*) was identified as an activator for the tapetum degeneration during pollen development (Li et al. 2011b). Within the anther, microspore mother cells undergo meiosis to produce male gametophytes, which then develop to mature pollen. Defects in meiotic process usually result in abnormal microgametogenesis, which then affects plant fertility. Through generation of numerous rice mutant libraries, genes related to the meiotic process and required for proper fertility in rice have been characterized. *PAIR1* and *PAIR3* are two novel gene encoding a putative coiled-coil protein that have been determined to be essential for the homologous chromosome pairing in rice (Nonomura et al. 2004a; Yuan et al. 2009), and *PAIR2*, an ortholog of *Arabidopsis ASY1* (Armstrong et al. 2002), has been shown to be required for homologous chromosome synapsis in meiosis I (Nonomura et al. 2004b, 2006).

OsRAD21-4 has a crucial role in chromosome condensation, subsequent pairing and synapsis, and separation of chromatids (Zhang et al. 2006b). *OsRPA1a* is required for DNA repair during meiosis and its knock-down mutants have shown low fertility (Chang et al. 2009). ZEP1, a transverse filament (TF) protein, is the rice homolog of *Arabidopsis thaliana* ZYP1. ZEP1 is the central element of the synaptonemal complex and regulates the number of crossovers during meiosis in rice (Wang et al. 2010b). Kinesin-1 family member *Pollen Semi-Sterility1* (*PSS1*) is essential for male meiotic chromosomal dynamics, male gametogenesis, and anther dehiscence in rice (Zhou et al. 2011).

In this study, we report the cloning and functional characterization of a novel WD40 motif-containing gene *lissencephaly type-1-like 1* (*OsLIS-L1*) in rice. Two independent mutant alleles, designated *oslis-l1-1* and *oslis-l1-2*, were identified from our T-DNA insertional mutant library (Wu et al. 2003; Zhang et al. 2006a, 2007) and POSTECH, South Korea (Jeon et al. 2000; Jeong et al. 2006), respectively. The two allelic mutants exhibited similar abnormal development phenotypes, such as semi-dwarf, shorter panicle length, and very low fertility. By introducing the *OsLIS-L1* genomic fragment into *oslis-l1-2* background, we successfully rescued the wild-type (WT) phenotypes, confirming *OsLIS-L1* was required for normal fertility in rice. Gene expression profile examination revealed that *OsLIS-L1* was relatively highly expressed in stem and panicles, consistent with its function in the cell development in stem and requirement for panicle development. During the panicle developmental process, *OsLIS-L1* showed a dynamic expression pattern in consecutive panicle developmental stages. Male meiocyte cytological examination suggested that *OsLIS-L1* does not affect the meiosis in pollen mother cells. Histological analysis revealed that the very low fertility was due to the abnormal male gametophyte formation. Histological analysis revealed that OsLIS-L1 regulates the cell proliferation in the first internode of the culms. Our results clearly indicate that *OsLIS-L1* is required for the cell elongation in the first internode and pollen development in rice.

Materials and methods

Plant materials and growth conditions

The *oslis-l1-1* (03Z11AI23) and *oslis-l1-2* (3A-04974) mutants were obtained from the Rice Mutant Database (RMD) (Wu et al. 2003; Zhang et al. 2006a; http://rmd.ncpgr.cn/) and the POSTECH Rice T-DNA Insertion Sequence Database (RISD) (Jeon et al. 2000; Jeong et al. 2006; http://www.postech.ac.kr/life/pfg/risd/), respectively. All plants were planted in the experimental field of Huazhong Agriculture University in Wuhan, China, during the rice-growing season of 2006–2010 with a planting density of 23 plants/m^2.

Genotyping of *oslis-l1* mutant plants

Polymerase chain reaction (PCR) genotyping of the *oslis-l1*-segregating population was performed by using the following primers: L1, R1 and NTLB5, L2, R2 and iAPL1, which are listed in Supplementary Table S1. PCR was conducted with an initial step of 94°C incubation for 5 min, followed by 30 cycles of 94°C for 45 s, 55°C for 45 s, and 72°C for 1 min; with a final extension at 72°C for 5 min.

Gene expression analysis

To extract total RNA of various tissues from Zhonghua 11 (*Oryza sativa* L. ssp. *japonica*), Trizol reagent (Invitrogen, Carlsbad, CA, USA) was used to isolate total RNA according to the manufacturer's instructions. Before the RNA reverse transcription step, total RNA was treated with amplification-grade DNase I (Invitrogen) for 15 min to degrade any residual genomic DNA. The synthesis of the cDNA first strand was carried out with Moloney Murine Leukemia Virus (M-MLV) reverse transcriptase (Promega Corp., Madison, WI, USA) according to the manufacturer's instructions. An aliquot (1 μl) of the reaction mixture was used for PCR. The PCR was performed in an ABI 9700 thermocycler (Applied Biosystem, Foster City, CA, USA) with three replicates. The cycling profile was as follows: 94°C for 5 min; 28 cycles at 94°C for 45 s, 55°C for 45 s, and 72°C for 1 min; and 72°C for 5 min. Next, 20 μl of the PCR product was separated in a 1.0% agarose gel and stained with ethidium bromide for visualization. The primer pairs used for reverse transcription (RT)-PCR were OsLIS-L1RT-L1 and OsLIS-L1RT-R1, OsLIS-L1RT-L2 and OsLIS-L1RT-R2, OsLIS-L1RT-L3 and OsLIS-L1RT-R3, and OsLIS-L1RT-L4 and OsLIS-L1RT-R4. *GAPDH* was used as the standard in all RT-PCR assays. qRT-PCR was performed in an optical 96-well plate that included 12.5 μl SYBR Premix EX Taq and 0.5 μl Rox Reference Dye II (Takara), 1 μl the cDNA sample, and 0.5 μl of each gene-specific primer, in a final volume of 25 μl on a PRISM 7500 PCR instrument (Applied Biosystems). The reactions were performed at 95°C for 30 s, 40 cycles of 95°C for 5 s, and 60°C for 34 s. Disassociation curve analysis was performed as follows: 95°C for 15 s, 60°C for 1 min, and 95°C for 15 s. Data were collected using the ABI PRISM 7500 sequence detection system following the instruction manual. The rice Ubiquitin5 gene was used as the internal control. All primers for RT-PCR and qRT-PCR are listed in Supplementary Table S1.

Vector construction and rice transformation

An approximately 12.2-kb genomic DNA fragment containing the entire *OsLIS-L1* coding region and the 1.4-kb upstream and 3.2-kb downstream sequence was obtained by *Nhe*I digestion from the Clemson BAC clone a0023F18. The fragment was inserted into the binary vector pCAMBIA2301 to generate the transformation plasmid pC2301–OsLIS-L1 for the complementation test.

To generate the *OsLIS-L1* RNAi vector, a 531-bp fragment was amplified with primers RNAi-L and RNAi-R (restriction sites added for subsequent cloning are underlined in Supplementary Table S1) from FL-cDNA clone AK111830 (http://cdna01.dna.affrc.go.jp/cDNA) and inserted into the pDS1301 vector as described (Chu et al. 2006). The two binary plasmids were introduced into *A. tumefaciens* EHA105 by electroporation, and the rice transformation was done according to the method of (Wu et al. 2003).

For expression in protoplasts, the full length open reading frame (ORF) of *OsLIS-L1* was amplified from FL-cDNA clone AK111830 (http://cdna01.dna.affrc.go.jp/cDNA) by PCR with the following primers: SC-L and SC-R (the *Xba*I restriction site is shown as the underlined sequence in Supplementary Table 1). The PCR product was cloned into pM999 vector containing the yellow fluorescence protein (YFP) reporter. Plasmids were purified using Qiagen (Valencia, CA, USA) columns according to the manufacturer's protocol. The plasmids were introduced into *Arabidopsis* protoplasts (prepared from leaf tissues) by polyethylene glycol-mediated transformation (Yoo et al. 2007). The reported rice transcription factor Ghd7 from our lab (Xue et al. 2008) was used as a reference for nuclear localization. Expression of the fusion construct was monitored at 36 h after transformation, and images were captured with the confocal microscope DMIRE2 (Leica, Germany).

Histochemical assays and microscopic analyses

Spikelets of various anther development stages were fixed in a solution containing 50% ethanol, 5% acetic glacial and 3.7% formaldehyde for 24 h at room temperature, and then replaced with 70% ethanol twice, and fixed anthers were dehydrated through an ethanol series, embedded into Technovit 7100 resin (Heraeus Kulzer), and polymerized at 37°C for 3 days. The sample blocks were sectioned into 2-μm-thick slices with a Leica microtome (Leica, Germany), sections were stained with 0.25% toluidine blue O (Merck), and the microscopic images were captured by a Leica DFC480 Digital Camera system (Leica, Germany).

For TEM, anthers at various developmental stages were prefixed with 2.5% glutaraldehyde in 0.1 M sodium phosphate buffer (pH 7.4), and were then fixed in 2% OsO_4 in phosphate-buffered saline (pH 7.4). Following ethanol dehydration, samples were embedded in epoxy resin (London Resin Company). Ultrathin sections (70 nm) were obtained using a UC6 ultramicrotome (Leica) and were then double stained with 2% (w/v) uranyl acetate and 2.6% (w/v) lead citrate aqueous solution. Observation and capturing of images were performed with an H-7650 transmission electron microscope (Hitachi) at 80 kV and an 832 charge-coupled device camera (Gatan).

Meiotic chromosome observation

The young panicles at meiosis stage were fixed with 5:3:2 of 95% ethanol:glacial acetic acid:chloroform for 24 h at room temperature, placed in 70% ethanol twice, and stored in 70% ethanol at 4°C until observation. The anthers were gently dissected with needles and afterward transferred to a glass slide together with a drop of improved carbol fuchsin. They were then opened gently with a needle to release pollen mother cells, anther wall debris was carefully removed, and a coverslip was added. Finally, the preparation was gently squashed by vertical thumb pressure under a double layer of filter paper and photographed with a Leica DFC480 (Leica, Germany) digital camera system. Images were enhanced with Photoshop CS.

Results

Morphological characterization of the *oslis-l1* mutant

We previously generated a rice T-DNA insertional mutant library with over 120,000 available independent lines and with 30,000 known T-DNA insertion sites (Wu et al. 2003; Zhang et al. 2006a, 2007). By screening T_1 plants from the tagged population, we identified a mutant *oslis-l1-1* that showed retarded vegetative growth and fertility defects. At the harvest stage, the height of the *oslis-l1-1* mutant plants was only 48.9 cm, whereas WT plants had a height of 87.3 cm (Fig. 1a; Table 1). The semi-dwarf phenotype of *oslis-l1-1* was partially due to its panicle length being shortened to 12.1 cm from 20.5 cm in WT (Fig. 1b; Table 1). The retarded vegetative growth also accompanied by smaller florets (Fig. 1c, d) and very low fertility. In contrast to the WT seed-setting rate (81.4%), the seed-setting rate of *oslis-l1-1* mutant was only 11.3% in the same normal field conditions (Table 1). The 10-seed length and width of *oslis-l1-1* was only 84.9 and 70.4% of the WT, respectively (Fig. 1e, f; Table 1). The segregation between normal and mutant plants in T_1 generation consistent with a Mendelian 3:1 ratio (normal:mutant = 16:4, $\chi^2 = 0.267$ for 3:1), suggesting a recessive mutation in single Mendelian locus controlled the phenotypes.

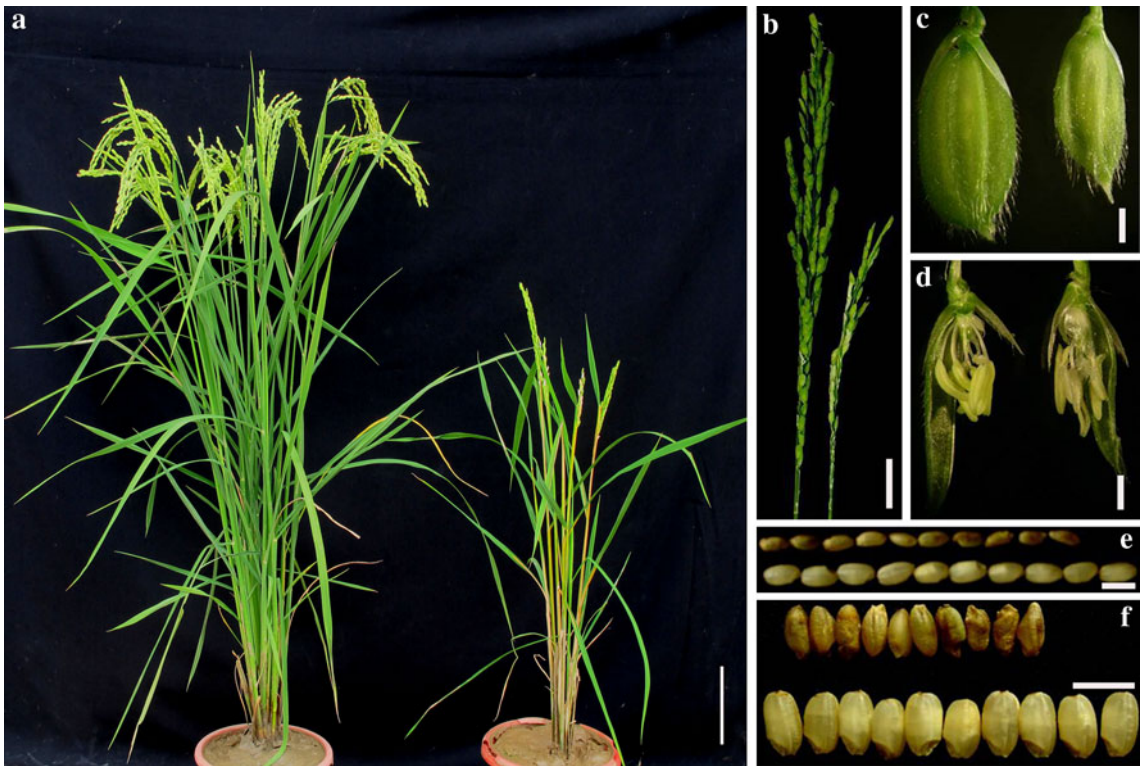

Fig. 1 Morphological characterization of wild-type (WT) and *oslis-l1-1* mutant plants. **a** A WT plant (*left*) and an *oslis-l1-1* mutant plant (*right*) at heading stage. *Bar* 10 cm. **b** A WT panicle (*left*) and an *oslis-l1-1* mutant panicle (*right*) at heading stage. *Bar* 2 cm. **c** A WT spikelet (*left*) and an *oslis-l1-1* (*right*) mutant spikelet before flowering. **d** A WT spikelet (*left*) and an *oslis-l1-1* (*right*) mutant spikelet after removing the lemma before flowering. *Bars* 1 mm in **c** and **d**. **e** Ten *oslis-l1-1* mutant grains length (*top*) and ten WT grains length (*bottom*). **f** Ten *oslis-l1-1* mutant grains width (*top*) and ten WT grains width (*bottom*). *Bars* 5 mm in **e** and **f**

T-DNA insertion occurs in a lissencephaly type-1-like gene that encodes a protein with WD40-repeat domain

To characterize the T-DNA insertion site of *oslis-l1-1*, we amplified the sequence flanking the T-DNA insertion using the thermal asymmetric interlaced-PCR technique (Zhang et al. 2007). The sequencing result of the PCR fragment revealed that T-DNA was inserted in the 21st intron of a gene that was located on chromosome 8 (Fig. 2a). The predicted transcript of the tagged gene was 7,617 bp, including a 3,402-bp coding sequence. The locus name of this gene had been registered as LOC_Os08g06480 in The Rice Genome Annotation Project (http://rice.plantbiology.msu.edu/). The gene of LOC_Os08g06480 was annotated encoding a lissencephaly type-1-like homology motif protein, thus we named it *OsLIS-L1* (*lissencephaly type-1-like 1*). *OsLIS-L1* comprised 25 exons and 24 introns (Fig. 2a). SMART algorithm analysis (http://smart.embl-heidelberg.de/) indicated that OsLIS-L1 contains four recognizable structural domains: starting from the N terminus, they are the LisH, CTLH, the domain with five WD40 repeats in the middle, and the domain with four WD40 repeats homologous to the β subunit of trimeric G-proteins (G_{β}) (Fig. 2e). The predicted protein encoded by the tagged gene contains 1,133 amino acid residues with a molecular mass of 124.8 kDa.

To test whether the abnormal phenotype could be attributable to T-DNA insertion in the LOC_Os08g06480 locus, a co-segregation test of the T-DNA tag with the

Table 1 Comparison of agronomic traits of *oslis-l1* mutants and their WT controls under normal field growth conditions (Wuhan, China, 2009)

Plants	Plant height (cm)	Panicle length (cm)	Pollen viability (%)	Seed setting (%)	10 seeds length (cm)	10 seeds width (cm)
OsLIS-L1-1	87.3 ± 2.5	20.5 ± 2.3	91.3 ± 10.7	81.4 ± 11.8	5.3 ± 0.4	2.7 ± 0.2
oslis-l1-1	48.9 ± 1.8	12.1 ± 0.87	27.1 ± 6.7	11.3 ± 5.1	4.5 ± 0.3	1.9 ± 0.3
OsLIS-L1-2	91.6 ± 4.1	22.9 ± 1.6	88.4 ± 9.6	71.8 ± 10.5	5.1 ± 0.2	2.8 ± 0.3
oslis-l1-2	63.1 ± 3.8	16.8 ± 2.1	8.1 ± 3.5	6.4 ± 5.1	5.0 ± 0.3	2.6 ± 0.2

The data correspond to the mean ± standard error from 10 individuals

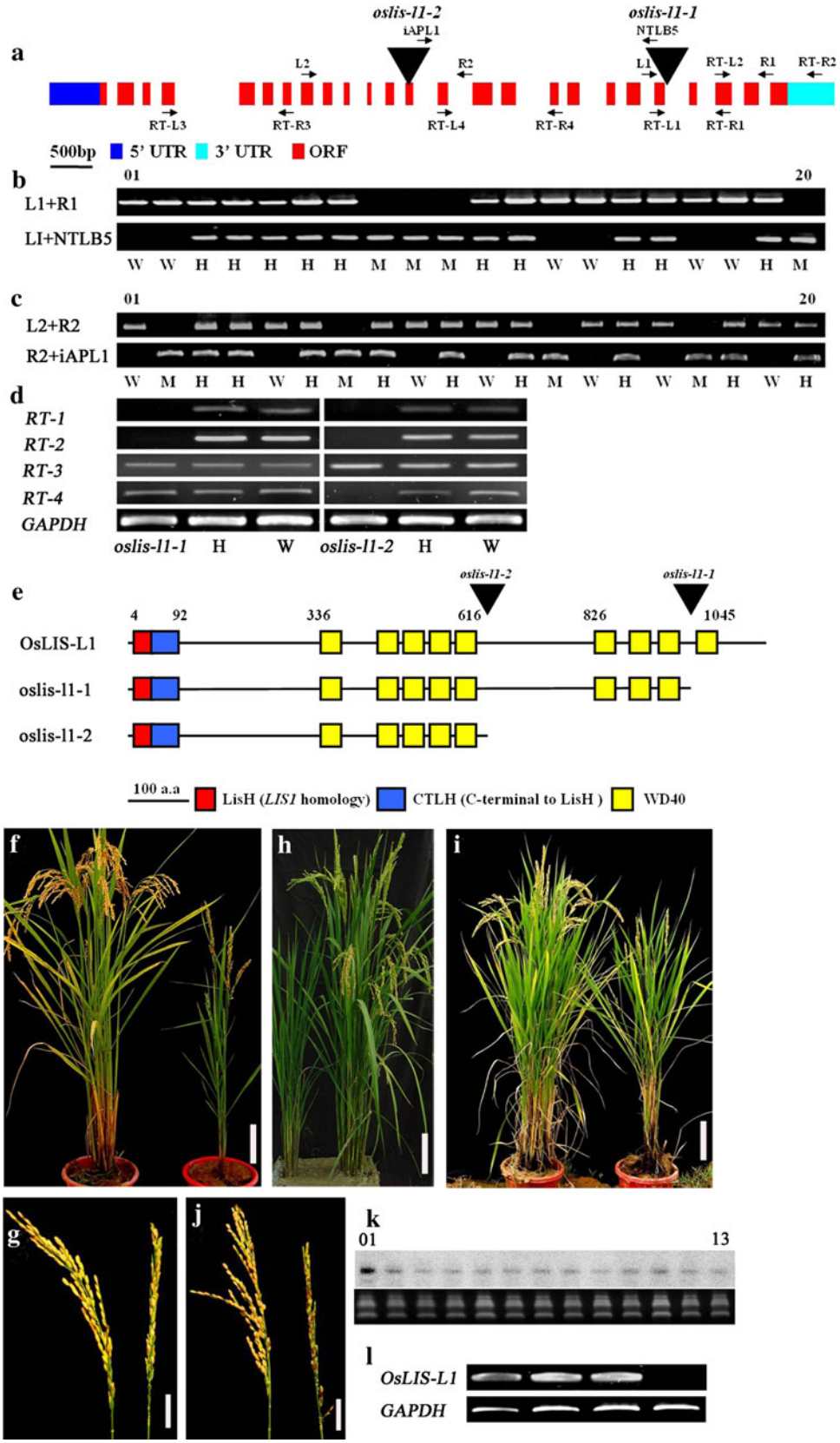
a
oslis-l1-2
iAPL1
oslis-l1-1
NTLB5
L2
R2
L1
RT-L2
R1
RT-R2
RT-L3
RT-R3
RT-L4
RT-R4
RT-L1
RT-R1
500bp
5' UTR
3' UTR
ORF
b
01
20
L1+R1
LI+NTLB5
W W H H H H H M M M H H W W H H W W H M
c
01
20
L2+R2
R2+iAPL1
W M H H W H M H W H W H M W H W M H W H
d
RT-1
RT-2
RT-3
RT-4
GAPDH
oslis-l1-1 H W oslis-l1-2 H W
e
oslis-l1-2
oslis-l1-1
4
92
336
616
826
1045
OsLIS-L1
oslis-l1-1
oslis-l1-2
100 a.a
LisH (LIS1 homology)
CTLH (C-terminal to LisH)
WD40
f
h
i
g
j
k
01
13
l
OsLIS-L1
GAPDH

◀ **Fig. 2** Molecular analysis of the *oslis-l1* mutants and RNAi transgenic plants, and the genetic complementation test. **a** Structure of the *OsLIS-L1* gene, position of T-DNA insertion, PCR and RT-PCR primers. *Red boxes* indicate exons encoding the protein, and *blue box* and *azure box* indicate the 5′ and 3′ UTR regions, respectively. *Arrows* identify primers for genotyping T-DNA insertion and RT-PCR. **b** Confirmation of co-segregation of T-DNA insertion with *oslis-l1-1* mutant phenotype in 20 T_1 plants. *Lanes* 8, 9, 10, and 20 are homozygous (*M*) which show mutant phenotype; *lanes* 3, 4, 5, 6, 7, 11, 12, 15, 16, and 19 are heterozygous (*H*) which show normal phenotype; and *lanes* 1, 2, 13, 14, 17, and 18 are WT (*W*) which show normal phenotype. **c** Confirmation of co-segregation of T-DNA insertion with *oslis-l1-2* mutant phenotype in 20 T_1 plants. *Lanes* 2, 7, 13, and 17 are homozygous (*M*) which show mutant phenotype; *lanes* 3, 4, 6, 8, 10, 12, 15, 18, and 20 are heterozygous (*H*) which show normal phenotype; and *lanes* 1, 5, 9, 11, 14, 16, and 19 are WT (*W*) which show normal phenotype. **d** RT-PCR analysis of *OsLIS-L1* expression by 4 pairs of RT-PCR primers in leaves from WT, heterozygous (*H*) and *oslis-l1* and *oslis-l1-2* at the seeding stage, respectively. **e** Structure of the whole transcript and 2 different truncated transcripts of *OsLIS-L1*. **f** A WT plant (*left*) and an *oslis-l1-2* mutant plant (*right*) at heading stage. **g** A WT panicle (*left*) and an *oslis-l1-2* panicle (*right*) at heading stage. **h** A positive pDS1301-OsLIS-L1 transgenic plant (*left*) and a negative pDS1301-OsLIS-L1 transgenic plant (*right*) at heading stage. **i** A positive pC2301–OsLIS-L1 transgenic plant (*left*) and a negative pC2301–OsLIS-L1 transgenic plant (*right*) at heading stage. *Bars* 10 cm in **f**, **h**, and **i**. **j** A positive pC2301–OsLIS-L1 transgenic plant panicle (*left*) and a negative pC2301–OsLIS-L1 transgenic plant panicle (*right*) at heading stage. *Bars* 2 cm in **g** and **j**. **k** Northern blot analysis, with 10 μg of total RNA used in each sample, and a region of *OsLIS-L1* serving as a probe. At *bottom* are the control ribosomal RNAs. A negative transgenic plant (*lane 1* in the gel) was used as control, and others are the positive transgenic plants. **l** RT-PCR analysis of *OsLIS-L1* expression in leaves from three positive pC2301–OsLIS-L1 transgenic plants (*first three lanes*) and a negative pC2301–OsLIS-L1 transgenic plant (*last lane*) at the seeding stage. Amplification of *GAPDH* cDNA was used to ensure that approximately equal amounts of cDNA were loaded

mutant phenotype was performed by PCR analysis of T_1 and T_2 plants. As shown in Fig. 2b, a combination of PCR results of primer set L1 + R1 and L1 + NTLB5 enable us to easily determine the genotype of plants in the T-DNA insertion site. Among the 20 T_1 plants we tested, all 4 T-DNA homozygous plants showed semi-dwarf and very low fertility phenotypes, whereas the T-DNA heterozygous and negative plants grew normally. In T_2 progeny, we examined more than 1,000 plants and all the T-DNA homozygous plants were semi-dwarf and had low fertility, whereas heterozygous plants and WT plants showed a normal phenotype (data not shown). These results showed that the semi-dwarf and low-fertility mutant phenotype was co-segregated with the T-DNA insertion in *OsLIS-L1*.

Loss-of-function of *OsLIS-L1* deduced the defects in *oslis-l1* mutants

To verify that the phenotypes in *oslis-l1-1* were due to the mutation of *OsLIS-L1*, we ordered an allelic mutant (3A-04974), which we designated as *oslis-l1-2*, from POSTECH, South Korea (Jeon et al. 2000; Jeong et al. 2006). *oslis-l1-2* harbored a T-DNA insertion in the 13th exon of *OsLIS-L1* (Fig. 2a). Using the same strategy as for *oslis-l1-1*, we confirmed the genotyping of *oslis-l1-2*, and the mutant phenotypes co-segregated closely with the T-DNA insertion (Fig. 2c). The mutant *oslis-l1-2* was also semi-dwarf with a shorter panicle length and low fertility, similar to that of *oslis-l1-1* (Fig. 2f, g; Table 1).

In order to verify *OsLIS-L1* function, we also generated *OsLIS-L1* RNAi-suppressed lines in WT background. An RNA blot experiment was employed to detect the *OsLIS-L1* transcript abundance in the RNAi-suppressed lines. Among the 37 positive transgenic lines, 12 of the plants showed *OsLIS-L1* expression level decreased to various extents (Fig. 2k). As expected, all the 12 RNAi-suppressed lines exhibited semi-dwarf height, shortened panicles, and low fertility, which mimicked the same defects with the two allelic T-DNA insertional mutants (Fig. 2h). Additionally, a genetic complementation experiment was performed to further confirm *OsLIS-L1* biological function. A construct pC2301–OsLIS-L1, containing the entire *OsLIS-L1* ORF, 1.4 kb upstream sequences, and a 3.2 kb downstream region, was introduced into *oslis-l1-2* mutant background by *Agrobacterium tumefaciens*-mediated transformation (Wu et al. 2003). Of the 20 independent transgenic plants generated, 15 restored normal fertility and plant height (Fig. 2i, j), whereas the other negative transgenic plants remained semi-dwarf and low-fertility phenotype similar to that of *oslis-l1-1* and *oslis-l1-2*. RT-PCR analysis showed that the transcripts of *OsLIS-L1* in leaves were also restored to the WT level in the positive transgenic plants, while the negative transgenic plants still showed no detectable *OsLIS-L1* expression as the mutant background (Fig. 2l). Next, we investigated the detail agronomic traits of the 20 T_0 generation complemented *oslis-l1* lines with pC2301–OsLIS-L1 (Supplemental Fig. 1a–d). In the progeny of the rescued plants, segregation of pC2301–OsLIS-L1 coincided with normal fertility, panicle length, and plant height (Supplemental Fig. 1e). All these results strongly showed that the *oslis-l1* mutant phenotypes were caused by the loss of *OsLIS-L1* function.

Different truncated *OsLIS-L1* transcripts generated in the two *oslis-l1* mutants

To check the effect of T-DNA insertions in *OsLIS-L1* at the mRNA level, we carried out RT-PCR with various primer sets (Fig. 2a). In *oslis-l1-1*, *OsLIS-L1* expression was not detectable when primer set RT1, which covered the *oslis-l1-1* T-DNA insertion site, was used for RT-PCR (Fig. 2d). The same result was found in primer set RT-2 analysis, which focused on the region downstream of T-DNA

insertion site (Fig. 2d). Interestingly, by using the primer sets RT-3 and RT-4, we found that the 5′ region of T-DNA insertion was normally transcribed in *oslis-l1-1* suggesting that T-DNA insertion in *oslis-l1-1* only partially destroyed the 3′ region of T-DNA insertion site and generated a truncated transcript (Fig. 2d, e). Similarly, we also found the same effect of T-DNA insertion on *oslis-l1-2* mRNA in that the 5′ region of T-DNA insertion was normally transcribed (Fig. 2d, e). As shown in Fig. 2a, e, T-DNA was located in the G_{β}-protein homology domain in *oslis-l1-1*, whereas the *oslis-l1-2* T-DNA inserted in the space between the five WD40-repeat domain and G_{β}-protein homology domain. Therefore, the two different truncated *OsLIS-L1* transcripts contained either a disrupted or a defective G_{β}-protein homology domain in two allelic mutants, suggesting that the integrity of G_{β}-protein homology domain is critical for OsLIS-L1 functions.

OsLIS-L1 does not affect the meiosis in pollen mother cells

Using the meiotic chromosome spreading method, we took *oslis-l1-2* as an example for observing chromosomal behavior during the meiosis process of the pollen mother cells to examine whether meiosis was abnormal. We emphasized on examining the homologous chromosome pairing, synapsis, and the integrity as in our previous studies (Chang et al. 2009; Yuan et al. 2009). In meiosis prophase I, from leptotene to diplotene, the chromosomes underwent condensation, synapse and pairing. Compared with WT, no obvious differences were detected in *oslis-l1-2* for those stages (Supplemental Fig. 2a–h). At diakinesis, chromosomes condensed to produce 12 bivalents, which were clearly observed both in *oslis-l1-2* and WT (Supplemental Fig. 2i, j). Thereafter, the bivalents aligned themselves along the equatorial plane at metaphase I (Supplemental Fig. 2k, l). At anaphase I, the homologous chromosome separated equationally and then generated dyads (Supplemental Fig. 2m, n). Through metaphase II, two groups of chromosomes separated equationally and produced tetrad spores (Supplemental Fig. 2o, p). During those stages, there were no obvious differences between *oslis-l1-2* and WT. There are equal division of univalents, normal formation of dyads and tetrads, and no DNA breakage during male meiocyte formation in *oslis-l1-2*. Our preliminary data indicated that the *oslis-l1* mutations did not affect chromosomal behavior during meiosis in pollen mother cells.

Abnormal male gametophyte formation in *oslis-l1* mutants

Since *oslis-l1-1* and *oslis-l1-2* mutant plants both exhibited a very low fertility phenotype, we next checked the mature pollen viability of *OsLIS-L1* mutants along with that of the WT by iodium potassium iodide staining assay. We found that 88.4% of the WT plant pollen was viable, with a regular round shape and dark staining under microscope (Fig. 3a). However, only about 27.1 and 8.1% of the *oslis-l1-1* and *oslis-l1-2* pollen, respectively, was dark stained (Fig. 3b; Table 1). In addition, *OsLIS-L1*-RNAi suppressed lines showed a faint staining similar to that of *oslis-l1* (Fig. 3c), and complementary transgenic plants showed normal dark stained (Fig. 3d). We also examined the *oslis-l1-2* male and female gamete fertility by reciprocal crosses between *oslis-l1-2* and WT plants. The seed-setting rates was 5.0, 7.0, and 7.9% in three independent panicles, using WT plants as maternal recipient pollinated with *oslis-l1-2* pollen. When using *oslis-l1-2* plants as maternal recipient pollinated with WT pollen, the seed-setting rates was 45.5, 49.3, and 54.6% in three independent panicles, the seed-setting rates were similar to those of reciprocal crosses between WT and WT plants. These results indicated that the *oslis-l1* mutant was almost female fertile and abnormal pollen may be the predominant reason for the low fertility in *oslis-l1* mutants.

To characterize the male sterility of the *oslis-l1* mutants, we compared the different development stages of the anthers in the WT and *oslis-l1-2* mutant plants by histological examination of plastic transverse sections. Recently, rice anther developments were further delineated into 14 stages (Zhang and Wilson 2009). From stages 1–5 (Fig. 3e, f), the microspore and the parietal cell development of *oslis-l1-2* was normal in WT as described previously. During these stages, the archesporial cells were divided to form primary parietal cells and primary sporogenous cells. The primary parietal cells then divided to form normal epidermis, endothecium, middle layer, and tapetum. During stages 6–8 (Fig. 3g–l), the microspore mother cells develop into tetrads thorough meiotic division. No obvious differences of anther cell wall and microspore mother cell development were observed from stages 5 to 8 between *oslis-l1-2* and WT (Fig. 3e–l).

Subsequently, at stage 9, there was still no obvious difference between WT and the *oslis-l1-2* anthers, microspores were released from tetrads, tapetal cells had deeply stained cytoplasm and the middle layer was hardly visible, and the middle layer appeared degenerated and almost invisible (Fig. 3m, n). At stage 10, the WT microspores appeared vacuolated and became round in shape (Fig. 3o), whereas the *oslis-l1-2* microspores had undersize and irregular vacuolation (Fig. 3p). At stage 11, the WT and the *oslis-l1-2* middle layer and endothecium degenerated, and typical falcate (sickle-like shape) pollen grains were formed in WT anthers (Fig. 3q), whereas *oslis-l1-2* produced severely abnormal pollen (Fig. 3r). At stage 12, during mature pollen formation, in the WT anther, mature pollen grains were deeply stained with 0.25% toluidine blue, indicating that the

WT microspore is full of starch, lipids, and other storage materials (Fig. 3s) that are required for pollen viability and function. However, in the *oslis-l1-2* anther, the pollen grains collapsed and consequently almost no normal pollen grains were released (Fig. 3t). During these stages, the middle layer and the tapetum are normally degenerated, and no obvious differences were observed in *oslis-l1-2* anthers compared to WT. Taken together, these findings suggest that the low fertility in *oslis-l1* might be due to the failure of normal microspore formation.

Next, we compared the anther cell wall development between the WT and *oslis-l1-2* at the level of ultra-structure using transmission electron microscopy (TEM). Consistent with the analysis for semi-thin sections of anthers, no obvious morphological changes were observed between anthers of the WT and *oslis-l1-2* from stages 9 to 12 (Supplemental Fig. 3a–h). The middle layer and the tapetum are normally degenerated, and the orbicules also normally formed. Furthermore, pollen wall development was not affected in *oslis-l1-2* compared with the WT anthers during stages 9–12 (Supplemental Fig. 3i–p). It seems that the pollen wall development is also not affected in *oslis-l1-2* mutants.

OsLIS-L1 controls stem growth by regulating cell proliferation

In order to characterize the semi-dwarf phenotype in *oslis-l1* mutant plants, we compared the length of five internodes from the main culms between the WT and *oslis-l1-2* mutant plants. Interestingly, we found that the length of the first internode under panicle differed the most between WT (32.1 cm) and *oslis-l1-2* mutant plants (22.1 cm), but there were no distinct differences between the lengths of other corresponding internodes (Fig. 4a, b; Table 2). Next, plastic transverse and longitudinal sections were employed to histologically analyze the first internode structure of the WT and *oslis-l1-2* mutant. The results showed that the stems of *oslis-l1-2* mutant plants consisted of the same layers and cells with the WT (Fig. 4c, d) and had the same stem thickness. Similarly, there was not much difference in cell size between the WT and *oslis-l1-2* mutant plants (Fig. 4e–g). Thus, we speculated that the decreased height of the stems in *oslis-l1* plants was mostly due to decreased cell proliferation rather than cell size in the first internode.

OsLIS-L1 is relatively highly expressed in stem and panicle and its protein localized in the nucleus

We examined the expression pattern of *OsLIS-L1* in various tissues and different developmental stages by quantitative RT (qRT)-PCR. As shown in Fig. 5a, the *OsLIS-L1* transcript had a relatively higher abundance in stem and panicles at the heading stage, though other tissues at the same stage such as root, leaf, and sheath, also showed weak expression of *OsLIS-L1*. This expression pattern of *OsLIS-L1* supported its function for internode elongation and panicle development in rice. Furthermore, we examined the dynamic *OsLIS-L1* expression pattern in various stages of panicle development by qRT-PCR. qRT-PCR was conducted on total RNA from different young panicle sizes (2.0–20.0 cm). *OsLIS-L1* transcripts were detected at a low level at P1 (2.0 cm). With the development of the panicle, *OsLIS-L1* transcripts increased and stayed relatively high from P2 to P6 (3.5–11.0 cm). Later, *OsLIS-L1* transcripts gradually faded out at P7 (16.5 cm) and P8 (20.0 cm) (Fig. 5a).

Most WD40-repeat proteins in plants are located in the nucleus (Han et al. 2006; Shi et al. 2005). To determine the subcellular localization of OsLIS-L1, OsLIS-L1 coding sequence was amplified and cloned into vector pM999 in appropriate ORF to fuse with YFP. Rice GHD7 is a known nuclear protein (Xue et al. 2008), and GHD7–CFP fusion protein was used as a marker in this experiment. By using an *Arabidopsis* mesophyll protoplasts transient gene expression system (Yoo et al. 2007), it was confirmed that the OsLIS-L1–YFP fusion protein was co-localized with the reported rice transcription factor GHD7 in the nucleus (Fig. 5b–e), suggesting that OsLIS-L1 is a nuclear protein.

Identification of *OsLIS-L1* ortholog in rice

BLAST searches revealed the existence of two homologues in rice: *Os01g15020* and *Os03g14980*. They possess very similar gene structure with *OsLIS-L1*. The annotated structure of *Os03g14980* and *OsLIS-L1* comprises of 25 exons and 24 introns, and *Os01g15020* comprises 24 exons and 23 introns (Supplemental Fig. 4a). The cDNA of *Os01g15020* and *Os03g14980* shared 36 and 39% nucleotide identity with *OsLIS-L1*, respectively; the Os01g15020 polypeptide shared 62% identity and the Os03g14980 polypeptide shared 67% identity with OsLIS-L1. SMART algorithm (http://smart.embl-heidelberg.de/) analysis of their polypeptide sequences indicated that they also contain four recognizable structural domains similar to OsLIS-L1: starting from the N terminus, they are the LisH, CTLH, the WD40-repeat domain in the middle, and the WD40-repeat domain at the C terminus (Supplemental Fig. 4b, c). The differences are that OsLIS-L1 has a five WD40-repeat domain in the middle, but Os01g15020 and Os03g14980 both have a six WD40-repeat domain in the middle, OsLIS-L1 and Os03g14980 both have a four WD40-repeat domain at the C terminus, whereas Os01g15020 has a five WD40-repeat domain at the C terminus. From the analysis above, the three genes were highly conserved during evolutions.

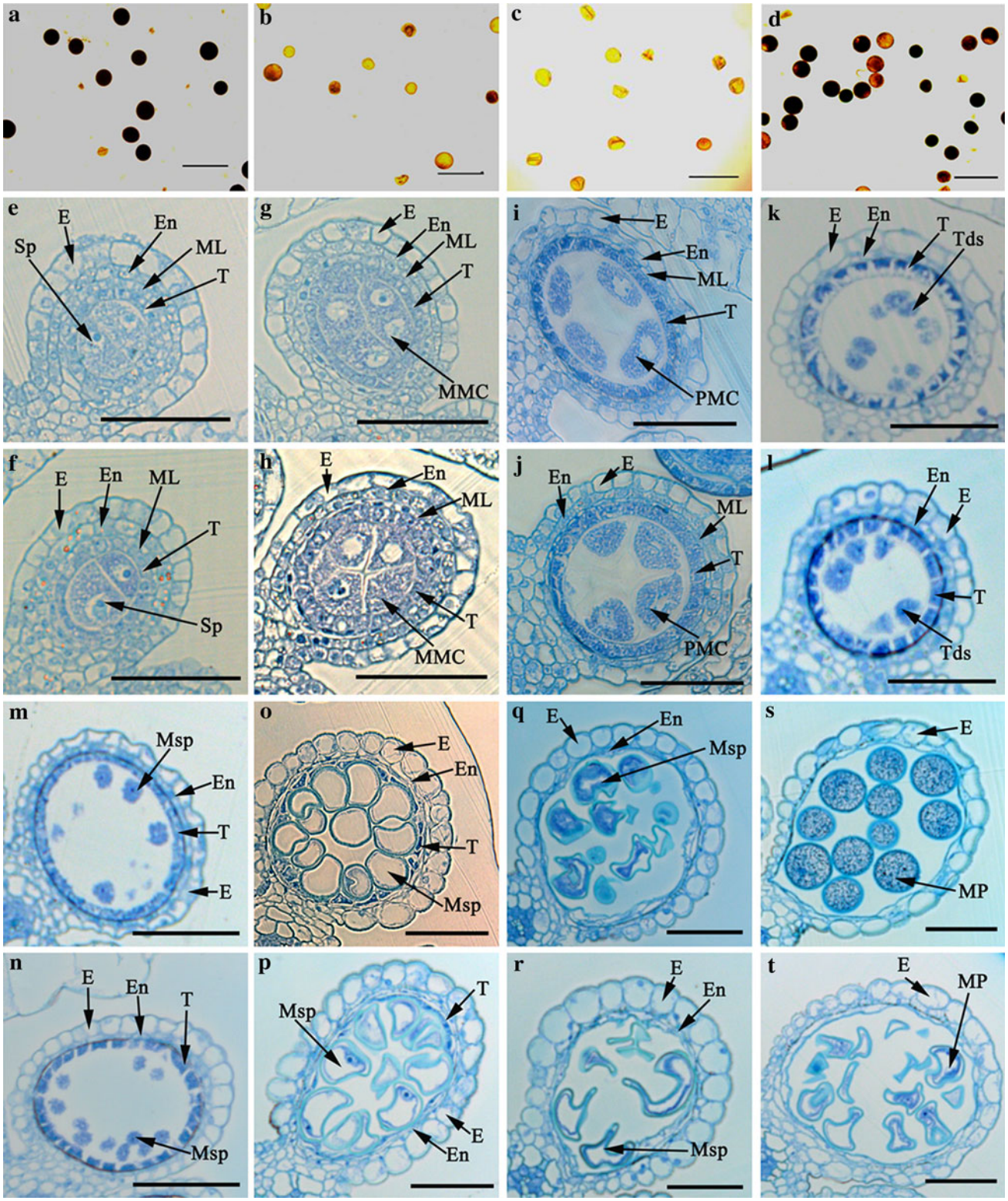
a
b
c
d
e
E
En
Sp
ML
T
g
E
En
ML
T
MMC
i
E
En
ML
T
PMC
k
E
En
T
Tds
f
E
En
ML
T
Sp
h
E
En
ML
T
MMC
j
En
E
ML
T
PMC
l
En
E
T
Tds
m
Msp
En
T
E
o
E
En
T
Msp
q
E
En
Msp
s
E
MP
n
E
En
T
Msp
p
T
Msp
E
En
r
E
En
Msp
t
E
MP

◀ **Fig. 3** Mature pollen viability by iodium potassium iodide staining assay and transverse section analysis of the anther development of the WT and the *oslis-l1-2* mutant. Mature pollen of WT (**a**), *oslis-l1-2* mutant (**b**), *OsLIS-L1* RNAi transgenic plants (**c**), and positive pC2301–OsLIS-L1 transgenic plant (**d**) were stained by iodium potassium iodide solution. *Bars* 125 μm. Cross sections of WT (**e**, **g**, **i**, **k**, **m**, **o**, **q**, **s**) and *oslis-l1-2* (**f**, **h**, **j**, **l**, **n**, **p**, **r**, **t**) at stage 5 (**e**, **f**), stage 6 (**g**, **h**), early stage 8 (**i**, **j**), late stage 8 (**k**, **l**), stage 9 (**m**, **n**), stage 10 (**o**, **p**), stage 11 (**q**, **r**), and stage 12 (**s**, **t**). *E* epidermis, *En* endothecium, *ML* middle layer, *MMC* microspore mother cell, *MP* mature pollen, *Msp* microspore, *PMC* pollen mother cell, *Sp* sporogenous cell, *T* tapetum, *Tds* tetrads. *Bars* 50 μm. All the plants were grown in the field under normal field growth conditions. Data were obtained from five individuals

To understand the expression patterns of the three genes, we extracted the expression data from the CREP database (http://crep.ncpgr.cn/; Wang et al. 2010a). The results from the database for 19 tissues of Minghui 63 (*O. sativa* L. ssp. *indica*) with two replications indicated that the three genes are expressed at different levels and exhibit a variety of expression patterns (Supplemental Fig. 4d). In general, *Os01g15020* and *Os03g14980* showed higher expression in the 19 tissues, but *OsLIS-L1* showed lowest expression in the 19 tissues. *OsLIS-L1* had a relatively higher expression in stem at the heading stage, 4–5 cm young panicle, and endosperm at 7 days after pollination. This expression pattern supported the fact that disruption of *OsLIS-L1* leads to semi-dwarf, low fertility, and smaller seeds phenotypes in rice (Fig. 1; Table 1). *Os03g14980* had high expression in the 19 tissues, with the highest expression level in endosperm at 21 days after pollination. *Os01g15020* showed a relatively higher expression in endosperm at 7 days after pollination and in flag leaf at 14 days after heading. Interestingly, all the three genes had relatively higher expression in endosperm at various stages, suggesting that they may be involved in the development of endosperm.

Discussion

G_β-protein homology domain plays an essential role for OsLIS-L1 function

As our study, the G_β-protein homology domain was either defected or disrupted in the two allelic mutants, while the other three domains, LisH, CTLH, and five WD40-repeat domain, were normally transcribed. This result suggested that G_β-protein homology domain is indispensable for OsLIS-L1 function in fertility and the first internode elongation. In *Arabidopsis*, a similar phenomenon was found in protein COP1 (McNellis et al. 1994). COP1 contains three recognizable structural domains: a zinc-binding motif in the N terminus, a putative coiled-coil region, and the domain with multiple WD40 repeats homologous to G_β in the C terminus. In total 17 available *COP1* recessive mutants were classified into three groups according to the severity of the phenotype. All three allelic *cop1* mutants with mutations in G_β-protein domain showed a lethal phenotype, suggesting that the integrity of G_β-protein domain is critical for COP1 functions. In addition, mutations in the region between the helical domain and the G_β-protein domain also seriously compromised the COP1 activity (McNellis et al. 1994). Our result in rice and COP1 result in *Arabidopsis* suggested a conservative function of G_β-protein domain with WD40 repeats in plants. The G_β-protein domain may affect OsLIS-L1 function in several possible ways. One possibility is that the loss of or defect in G_β-protein domain altered the OsLIS-L1 protein configuration, thus decreased the protein stability in plant cell. It is also possible that G_β-protein domain acts as a functional domain for certain biochemical activities, because several studies have shown that repeated WD40 motifs in G_β-protein domain may be involved in protein–protein interactions and serve as platforms for the assembly of protein complexes (Smith et al. 1999; Wang et al. 2001). Because of the lack of mutations in the LISH domain and five WD40-repeat domain, we could not study the possible functions of these two domains in OsLIS-L1 at this moment.

OsLIS-L1 profile indicates its function

The spatial and temporal expression pattern of a gene can be indicative of its functional relevance. A wide expression pattern of *OsLIS-L1* in different tissues and stages suggests that the gene may play crucial roles at multiple developmental stages. However, a relatively higher transcript level was detected in stem and panicles in mature rice plants by qRT-PCR (Fig. 5a). The plant height of *oslis-l1-1* and *oslis-l1-2* was reduced to 56.0 and 68.9% of WT, respectively (Table 1). The decreased seed-setting rate in both *oslis-l1* mutants also coincided with the high *OsLIS-L1* expression level in panicle. Moreover, the transcript of *OsLIS-L1* was greatest through the panicle developmental stage P2–P6, which approximately represented stage 6–10. This expression pattern also supports our histological analysis result showing the failure of normal microspores formation in *oslis-l1-2*. The expression pattern of *OsLIS-L1* together with the phenotype observed in the *oslis-l1-1* and *oslis-l1-2* mutants indicated that the *OsLIS-L1* is required for male gametophyte generation.

OsLIS-L1 functions in male gametophyte formation in rice

In flowering plants, the male gametophyte development is very essential for sexual reproduction. The *oslis-l1-1* and *oslis-l1-2* mutant plants both exhibit very low fertility phenotypes (Table 1), and almost all the pollen lacked starch due

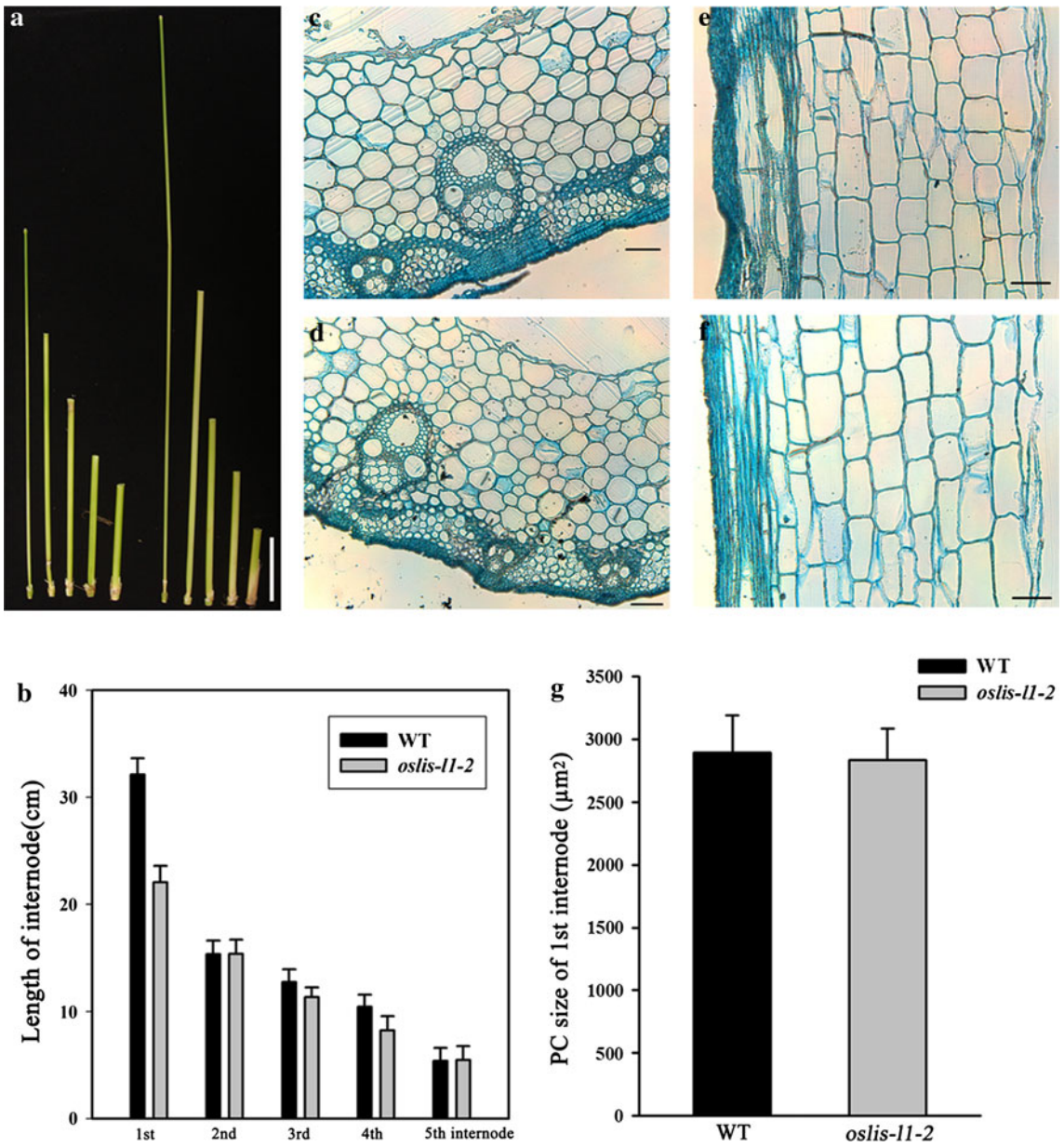

Fig. 4 Morphological characterization of *OsLIS-L1* on the stem. **a** The five internodes under panicle from the main culms at mature stage for the following (from *left* to *right*): the first internode of *oslis-l1-2*, the second internode of *oslis-l1-2*, the third internode of *oslis-l1-2*, the fourth internode of *oslis-l1-2*, the fifth internode of *oslis-l1-2*, and the first internode of WT, the second internode of WT, the third internode of WT, the fourth internode of WT, the fifth internode of WT. *Bar* 5 cm. **b** The length of the five internodes under panicle from the main culms between *oslis-l1-2* and WT at mature stage. The data correspond to the mean ± standard error from 20 individuals. **c** WT and **d** *oslis-l1-2* transverse sections of the first internode under panicle from the main culms at heading stage. **e** WT and **f** *oslis-l1-2* longitudinal sections of the first internode under panicle from the main culms at heading stage. *Bars* 50 μm in **c–f**. **g** Size of parenchyma cells (*PC*) in the first internode of WT and *oslis-l1-2*. The data correspond to the mean ± standard error from 15 individuals. All the plants grown in the field under normal field growth conditions

to failure of male gametophyte development. From male meiocyte meiosis analysis in the WT and *oslis-l1-2* mutant, there were no obvious differences during the meiosis process (Supplemental Fig. 2), suggesting that *OsLIS-L1* did not affect the meiosis in pollen mother cells. Based on the histological examination and TEM results of anther development in the WT and the *oslis-l1-2* mutant, there were no obvious differences in the four somatic layers and pollen wall during the male gametophyte generation (Fig. 3; Supplemental Fig. 3), indicating that OsLIS-L1 did not function in anther wall and pollen wall development and that the reduced male fertility phenotype was not due to defects in anther wall and pollen wall development. The obvious defects were clearly observed at the later stages of the anther

Table 2 Comparison of length of five internodes from the main culms between the wild-type and *oslis-l1-2* mutant plants under normal field growth conditions (Wuhan, China, 2009)

Plants	First internode (cm)	Second internode (cm)	Third internode (cm)	Fourth internode (cm)	Fifth internode (cm)
OsLIS-L1-2	32.1 ± 1.5	15.3 ± 1.3	12.7 ± 1.2	10.4 ± 1.2	5.4 ± 1.2
oslis-l1-2	22.1 ± 1.5	15.4 ± 1.3	11.3 ± 0.9	8.2 ± 1.3	5.5 ± 1.3

The data correspond to the mean ± standard error from 20 individuals

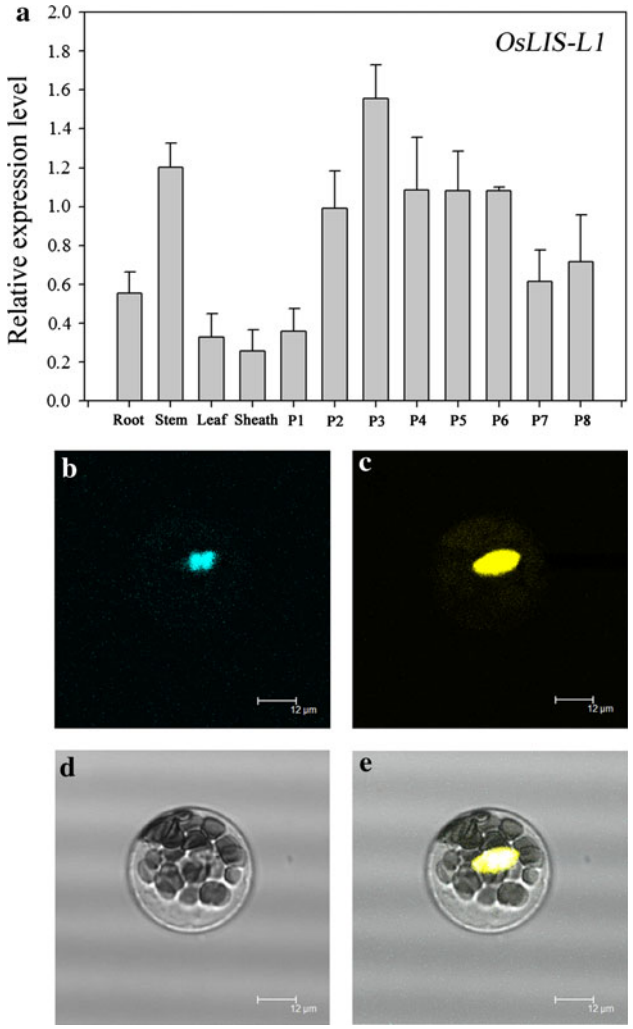

Fig. 5 *OsLIS-L1* expression pattern and its protein subcellular localization. **a** qRT-PCR analysis of *OsLIS-L1* expression levels in root, stem, leaf, and sheath at heading stage. Panicles at various developmental stages according to their length at heading stage (*P1–P8*). *P1* approximately 2.0 cm, *P2* approximately 3.5 cm, *P3* approximately 4.5 cm, *P4* approximately 6.5 cm, *P5* approximately 8.0 cm, *P6* approximately 11.0 cm, *P7* approximately 16.5 cm, *P8* approximately 20.0 cm, respectively. Ubiquitin5 was used as a control for normalization. The data shown are means ± SE from three biological repeats and two technical repeats. **b** Localization of Ghd7–CFP fusion protein. **c** Localization of OsLIS-L1–YFP fusion protein. **d** Image of the cell in bright field. **e** Merged image of **b–d**. *Bars* 12 μm in **b–e**

development. The *oslis-l1* pollen grains were severely collapsed and consequently no viable pollen grain were released (Fig. 3t). This is a different situation from that frequently reported in the literature in which male sterility is usually associated with defects in tapetum development or the meiotic process (Jung et al. 2006; Li et al. 2006, 2011b; Yuan et al. 2009). Our observation in *oslis-l1-2* is different from the other reported male sterile mutants in rice. For example, rice *Undeveloped Tapetum1* (*Udt1*) begins to function at the meiosis stage for tapetum development and pollen mother cell meiosis. Moreover, this gene is needed to degenerate the middle layer (Jung et al. 2005). Mutation of the rice gene *PAIR3* exhibits male sterile phenotype mostly due to abnormal male gametophyte formation and lack of bivalent formation in meiosis, but the cells of the parietal layer including the tapetum appeared to be normal (Yuan et al. 2009). The rice (*Oryza sativa*) *APOPTOSIS INHIBITOR5* (*API5*) regulates the development of male gametophytes through programmed cell death (PCD) during tapetum degeneration (Li et al. 2011b). Combining our present data, we speculate *OsLIS-L1* may be involved in the other developmental process for microsporogenesis. Thus, the functional details of *OsLIS-L1* on microsporogenesis still needs to be elucidated in future investigation.

The role of *OsLIS-L1* in the development of the first internode in rice

Plant height is an important agronomic trait that is related to lodging resistance and fertilizer endurance (Shan et al. 2009). Here, we identified *OsLIS-L1* was required for the first internode elongation but not for the other internodes of the culm in rice (Fig. 4a, b; Table 2). The semi-dwarf mutant phenotype of *oslis-l1* is quite different with other reporters in rice. For example, mutation of *OsH15*, *OsDHT8*, and *SPD6* exhibit dwarf phenotype mostly due to the decrease the length of the second, third, and fourth internodes, but the length of first internode was not distinctly different from that of WT plant (Sato et al. 1999; Shan et al. 2009; Wei et al. 2010). In some cases, the length of all the internodes were shortened, led to severe dwarf phenotype in *brd1* mutant plants (Mori et al. 2002).

The effect on different internodes may be a hint that these genes are involved in different pathways regulating vegetative growth in rice.

Recent studies revealed that defects in cell division and cell expansion are two major reasons for dwarf phenotype in plants (Kumar et al. 2010). Rice height was reported to be affected by *DTH8* or *OsHAP* complexes mainly through the regulation of internode cell elongation (Wei et al. 2010). In *OsAPC6* mutant plant, both the cell size and cell number were reduced (Kumar et al. 2010). Given that the *oslis-l1-2* first internode cell size was kept the same as that in WT (Fig. 4c–g), we speculated that the reduced plant height in *oslis-l1-2* plants was mostly due to a decreased cell proliferation. Sato et al. (1999) also observed reduction in the number of cells in internode in *OSH15* mutant in rice due to decreased frequency of cell proliferation in the intercalary meristem. A challenge for future studies will be to elucidate the molecular mechanisms controlling the cell proliferation in the fist internode in rice.

Acknowledgments We thank Dr. Jian Xu for providing the plasmid pM999 and Dr. Gynheung An for providing the T-DNA insertional line 3A-04974. We thank Dr. Meizhong Luo for providing the Zhonghua 11 genomic DNA BAC clone a0023F18. This research was supported by grants from Program for New Century Excellent Talents in University, the National Natural Science Foundation of China, and the Key Project on Plant Transgenic Research.

References

Armstrong SJ, Caryl AP, Jones GH, Franklin FC (2002) Asy1, a protein required for meiotic chromosome synapsis, localizes to axis-associated chromatin in *Arabidopsis* and *Brassica*. J Cell Sci 115:3645–3655

Chang Y, Gong L, Yuan W, Li X, Chen G, Zhang Q, Wu C (2009) Replication protein A (RPA1a) is required for meiotic and somatic DNA repair but is dispensable for DNA replication and homologous recombination in rice. Plant Physiol 151:2162–2173

Chen R, Zhao X, Shao Z, Wei Z, Wang Y, Zhu L, Zhao J, Sun M, He R, He G (2007) Rice UDP-glucose pyrophosphorylase1 is essential for pollen callose deposition and its cosuppression results in a new type of thermosensitive genic male sterility. Plant Cell 19:847–861

Chu Z, Yuan M, Yao J, Ge X, Yuan B, Xu C, Li X, Fu B, Li Z, Bennetzen JL, Zhang Q, Wang S (2006) Promoter mutations of an essential gene for pollen development result in disease resistance in rice. Genes Dev 20:1250–1255

Emes RD, Ponting CP (2001) A new sequence motif linking lissencephaly, Treacher Collins and oral-facial-digital type 1 syndromes, microtubule dynamics and cell migration. Hum Mol Genet 10:2813–2820

Franks RG, Wang C, Levin JZ, Liu Z (2002) SEUSS, a member of a novel family of plant regulatory proteins, represses floral homeotic gene expression with LEUNIG. Development 129:253–263

Han MJ, Jung KH, Yi G, Lee DY, An G (2006) Rice Immature Pollen 1 (RIP1) is a regulator of late pollen development. Plant Cell Physiol 47:1457–1472

Hoecker U, Tepperman JM, Quail PH (1999) SPA1, a WD-repeat protein specific to phytochrome A signal transduction. Science 284:496–499

Holm M, Ma LG, Qu LJ, Deng XW (2002) Two interacting bZIP proteins are direct targets of COP1-mediated control of light-dependent gene expression in *Arabidopsis*. Genes Dev 16:1247–1259

Hu L, Liang W, Yin C, Cui X, Zong J, Wang X, Hu J, Zhang D (2011) Rice MADS3 regulates ROS homeostasis during late anther development. Plant Cell 23:515–533

Huang J, Wang MM, Bao YM, Sun SJ, Pan LJ, Zhang HS (2008) SRWD: a novel WD40 protein subfamily regulated by salt stress in rice (*Oryza sativa* L.). Gene 424:71–79

Jeon JS, Lee S, Jung KH, Jun SH, Jeong DH, Lee J, Kim C, Jang S, Yang K, Nam J, An K, Han MJ, Sung RJ, Choi HS, Yu JH, Choi JH, Cho SY, Cha SS, Kim SI, An G (2000) T-DNA insertional mutagenesis for functional genomics in rice. Plant J 22:561–570

Jeong DH, An S, Park S, Kang HG, Park GG, Kim SR, Sim J, Kim YO, Kim MK, Kim J, Shin M, Jung M, An G (2006) Generation of a flanking sequence-tag database for activation-tagging lines in japonica rice. Plant J 45:123–132

Jung KH, Han MJ, Lee YS, Kim YW, Hwang I, Kim MJ, Kim YK, Nahm BH, An G (2005) Rice Undeveloped Tapetum1 is a major regulator of early tapetum development. Plant Cell 17:2705–2722

Jung KH, Han MJ, Lee DY, Lee YS, Schreiber L, Franke R, Faust A, Yephremov A, Saedler H, Kim YW, Hwang I, An G (2006) Wax-deficient anther1 is involved in cuticle and wax production in rice anther walls and is required for pollen development. Plant Cell 18:3015–3032

Kaya H, Shibahara KI, Taoka KI, Iwabuchi M, Stillman B, Araki T (2001) FASCIATA genes for chromatin assembly factor-1 in *Arabidopsis* maintain the cellular organization of apical meristems. Cell 104:131–142

Kim MH, Cooper DR, Oleksy A, Devedjiev Y, Derewenda U, Reiner O, Otlewski J, Derewenda ZS (2004) The structure of the N-terminal domain of the product of the lissencephaly gene Lis1 and its functional implications. Structure 12:987–998

Kumar M, Basha PO, Puri A, Rajpurohit D, Randhawa GS, Sharma TR, Dhaliwal HS (2010) A candidate gene OsAPC6 of anaphase-promoting complex of rice identified through T-DNA insertion. Funct Integr Genomics 10:349–358

Lee JH, Terzaghi W, Gusmaroli G, Charron JB, Yoon HJ, Chen H, He YJ, Xiong Y, Deng XW (2008) Characterization of *Arabidopsis* and rice DWD proteins and their roles as substrate receptors for CUL4-RING E3 ubiquitin ligases. Plant Cell 20:152–167

Li N, Zhang DS, Liu HS, Yin CS, Li XX, Liang WQ, Yuan Z, Xu B, Chu HW, Wang J, Wen TQ, Huang H, Luo D, Ma H, Zhang DB (2006) The rice tapetum degeneration retardation gene is required for tapetum degradation and anther development. Plant Cell 18:2999–3014

Li H, He Z, Lu G, Lee SC, Alonso J, Ecker JR, Luan S (2007) A WD40 domain cyclophilin interacts with histone H3 and functions in gene repression and organogenesis in *Arabidopsis*. Plant Cell 19:2403–2416

Li H, Pinot F, Sauveplane V, Werck-Reichhart D, Diehl P, Schreiber L, Franke R, Zhang P, Chen L, Gao Y, Liang W, Zhang D (2010) Cytochrome P450 family member CYP704B2 catalyzes the {omega}-hydroxylation of fatty acids and is required for anther cutin biosynthesis and pollen exine formation in rice. Plant Cell 22:173–190

Li H, Yuan Z, Vizcay-Barrena G, Yang C, Liang W, Zong J, Wilson ZA, Zhang D (2011a) PERSISTENT TAPETAL CELL1 encodes a PHD-finger protein that is required for tapetal cell death and pollen development in rice. Plant Physiol 156:615–630

Li X, Gao X, Wei Y, Deng L, Ouyang Y, Chen G, Li X, Zhang Q, Wu C (2011b) Rice APOPTOSIS INHIBITOR5 coupled with two DEAD-Box adenosine 5′-triphosphate-dependent RNA helicases regulates tapetum degeneration. Plant Cell 23:1416–1434

Liu Z, Meyerowitz EM (1995) LEUNIG regulates AGAMOUS expression in *Arabidopsis* flowers. Development 121:975–991

Ma H (2005) Molecular genetic analyses of microsporogenesis and microgametogenesis in flowering plants. Annu Rev Plant Biol 56:393–434

McNellis TW, von Arnim AG, Araki T, Komeda Y, Misera S, Deng XW (1994) Genetic and molecular analysis of an allelic series of cop1 mutants suggests functional roles for the multiple protein domains. Plant Cell 6:487–500

Mori M, Nomura T, Ooka H, Ishizaka M, Yokota T, Sugimoto K, Okabe K, Kajiwara H, Satoh K, Yamamoto K, Hirochika H, Kikuchi S (2002) Isolation and characterization of a rice dwarf mutant with a defect in brassinosteroid biosynthesis. Plant Physiol 130:1152–1161

Neer EJ, Schmidt CJ, Nambudripad R, Smith TF (1994) The ancient regulatory-protein family of WD-repeat proteins. Nature 371:297–300

Nonomura K, Nakano M, Fukuda T, Eiguchi M, Miyao A, Hirochika H, Kurata N (2004a) The novel gene HOMOLOGOUS PAIRING ABERRATION IN RICE MEIOSIS1 of rice encodes a putative coiled-coil protein required for homologous chromosome pairing in meiosis. Plant Cell 16:1008–1020

Nonomura KI, Nakano M, Murata K, Miyoshi K, Eiguchi M, Miyao A, Hirochika H, Kurata N (2004b) An insertional mutation in the rice PAIR2 gene, the ortholog of *Arabidopsis* ASY1, results in a defect in homologous chromosome pairing during meiosis. Mol Genet Genomics 271:121–129

Nonomura K, Nakano M, Eiguchi M, Suzuki T, Kurata N (2006) PAIR2 is essential for homologous chromosome synapsis in rice meiosis I. J Cell Sci 119:217–225

Reiner O, Carrozzo R, Shen Y, Wehnert M, Faustinella F, Dobyns WB, Caskey CT, Ledbetter DH (1993) Isolation of a Miller–Dieker lissencephaly gene containing G protein beta-subunit-like repeats. Nature 364:717–721

Reiner O, Sapoznik S, Sapir T (2006) Lissencephaly 1 linking to multiple diseases: mental retardation, neurodegeneration, schizophrenia, male sterility, and more. Neuromolecular Med 8:547–565

Sato Y, Sentoku N, Miura Y, Hirochika H, Kitano H, Matsuoka M (1999) Loss-of-function mutations in the rice homeobox gene OSH15 affect the architecture of internodes resulting in dwarf plants. EMBO J 18:992–1002

Shan JX, Zhu MZ, Shi M, Gao JP, Lin HX (2009) Fine mapping and candidate gene analysis of spd6 responsible for small panicle and dwarfness in wild rice (*Oryza rufipogon* Griff.). Theor Appl Genet 119:827–836

Shi DQ, Liu J, Xiang YH, Ye D, Sundaresan V, Yang WC (2005) SLOW WALKER1, essential for gametogenesis in Arabidopsis, encodes a WD40 protein involved in 18S ribosomal RNA biogenesis. Plant Cell 17:2340–2354

Smith TF, Gaitatzes C, Saxena K, Neer EJ (1999) The WD repeat: a common architecture for diverse functions. Trends Biochem Sci 24:181–185

Sondek J, Bohm A, Lambright DG, Hamm HE, Sigler PB (1996) Crystal structure of a G-protein beta gamma dimer at 2.1 Å resolution. Nature 379:369–374

Sorensen MB, Chaudhury AM, Robert H, Bancharel E, Berger F (2001) Polycomb group genes control pattern formation in plant seed. Curr Biol 11:277–281

Tai CY, Dujardin DL, Faulkner NE, Vallee RB (2002) Role of dynein, dynactin, and CLIP-170 interactions in LIS1 kinetochore function. J Cell Biol 156:959–968

Ullah H, Chen JG, Temple B, Boyes DC, Alonso JM, Davis KR, Ecker JR, Jones AM (2003) The beta-subunit of the Arabidopsis G protein negatively regulates auxin-induced cell division and affects multiple developmental processes. Plant Cell 15:393–409

van Nocker S, Ludwig P (2003) The WD-repeat protein superfamily in *Arabidopsis*: conservation and divergence in structure and function. BMC Genomics 4:50

von Arnim AG, Osterlund MT, Kwok SF, Deng XW (1997) Genetic and developmental control of nuclear accumulation of COP1, a repressor of photomorphogenesis in *Arabidopsis*. Plant Physiol 114:779–788

Wang H, Ma LG, Li JM, Zhao HY, Deng XW (2001) Direct interaction of *Arabidopsis* cryptochromes with COP1 in light control development. Science 294:154–158

Wang L, Xie W, Chen Y, Tang W, Yang J, Ye R, Liu L, Lin Y, Xu C, Xiao J, Zhang Q (2010a) A dynamic gene expression atlas covering the entire life cycle of rice. Plant J 61:752–766

Wang M, Wang K, Tang D, Wei C, Li M, Shen Y, Chi Z, Gu M, Cheng Z (2010b) The central element protein ZEP1 of the synaptonemal complex regulates the number of crossovers during meiosis in rice. Plant Cell 22:417–430

Wei X, Xu J, Guo H, Jiang L, Chen S, Yu C, Zhou Z, Hu P, Zhai H, Wan J (2010) DTH8 suppresses flowering in rice, influencing plant height and yield potential simultaneously. Plant Physiol 153:1747–1758

Wu C, Li X, Yuan W, Chen G, Kilian A, Li J, Xu C, Zhou DX, Wang S, Zhang Q (2003) Development of enhancer trap lines for functional analysis of the rice genome. Plant J 35:418–427

Xue W, Xing Y, Weng X, Zhao Y, Tang W, Wang L, Zhou H, Yu S, Xu C, Li X, Zhang Q (2008) Natural variation in Ghd7 is an important regulator of heading date and yield potential in rice. Nat Genet 40:761–767

Yoo SD, Cho YH, Sheen J (2007) *Arabidopsis* mesophyll protoplasts: a versatile cell system for transient gene expression analysis. Nat Protoc 2:1565–1572

Yuan W, Li X, Chang Y, Wen R, Chen G, Zhang Q, Wu C (2009) Mutation of the rice gene PAIR3 results in lack of bivalent formation in meiosis. Plant J 59:303–315

Zhang D, Wilson ZA (2009) Stamen specification and anther development in rice. Chin Sci Bull 54:2342–2352

Zhang J, Li C, Wu C, Xiong L, Chen G, Zhang Q, Wang S (2006a) RMD: a rice mutant database for functional analysis of the rice genome. Nucleic Acids Res 34:D745–D748

Zhang L, Tao J, Wang S, Chong K, Wang T (2006b) The rice OsRad21–4, an orthologue of yeast Rec8 protein, is required for efficient meiosis. Plant Mol Biol 60:533–554

Zhang J, Guo D, Chang Y, You C, Li X, Dai X, Weng Q, Chen G, Liu H, Han B, Zhang Q, Wu C (2007) Non-random distribution of T-DNA insertions at various levels of the genome hierarchy as revealed by analyzing 13 804 T-DNA flanking sequences from an enhancer-trap mutant library. Plant J 49:947–959

Zhang DS, Liang WQ, Yuan Z, Li N, Shi J, Wang J, Liu YM, Yu WJ, Zhang DB (2008) Tapetum degeneration retardation is critical for aliphatic metabolism and gene regulation during rice pollen development. Mol Plant 1:599–610

Zhang H, Liang W, Yang X, Luo X, Jiang N, Ma H, Zhang D (2010) Carbon starved anther encodes a MYB domain protein that regulates sugar partitioning required for rice pollen development. Plant Cell 22:672–689

Zhou S, Wang Y, Li W, Zhao Z, Ren Y, Gu S, Lin Q, Wang D, Jiang L, Su N, Zhang X, Liu L, Cheng Z, Lei C, Wang J, Guo X, Wu F, Ikehashi H, Wang H, Wan J (2011) Pollen semi-sterility1 encodes a kinesin-1-like protein important for male meiosis, anther dehiscence, and fertility in rice. Plant Cell 23:111–129